# 11

# Nanoscopic and Macroscopic Structuring of Covalent Organic Frameworks

## 11.1 Introduction

In Chapters 7–10 we have outlined how the existing toolbox of molecular organic chemistry can be applied to the construction and modification of crystalline porous extended organic solids. This chapter covers a challenge that emerges with the transition from solution-based molecular chemistry to the chemistry of insoluble solids such as covalent organic frameworks (COFs). We have highlighted the importance of crystallinity for the elucidation of the structure of COFs on the atomic level. This knowledge is crucial as it enables structure–function correlations and thus rational optimization of the material with respect to its structural properties (topology and structure metrics) and chemical properties (chemical stability of the linkage, appended functionality on the backbone). While crystallinity gives information about the long-range order on the atomic scale it is not strictly related to the nanoscopic or macroscopic morphology of the material. This is an important point to consider with respect to applications of heterogeneous materials where the morphology has a profound impact on the performance. COFs have received a lot of attention in the context of organic electronics because they exhibit high charge carrier mobility, are pseudocapacitive energy storage materials, and can be employed as electrocatalysts [1]. All of these applications benefit from nanostructured forms of COFs. In general, organic materials can be processed (e.g. thin films, crystals) from solution, but COFs, unlike conventional 1D polymers or molecular organic materials, are insoluble in common organic solvents or water and are generally isolated as aggregated microcrystalline powders. With regard to processing powder samples they can be exfoliated into dispersible few- or monolayer sheets by top–down approaches such as sonication, grinding, or chemical exfoliation. Alternatively, a bottom–up approach can be taken and controlled nucleation on substrates, polymerization at the liquid–liquid interface, flow chemistry, or the assembly on surfaces using chemical vapor deposition techniques in ultrahigh vacuum are being explored. In the following text, we will give an overview of synthetic strategies for structuring COFs and illustrate advantages and disadvantages of the respective approaches.

*Introduction to Reticular Chemistry: Metal-Organic Frameworks and Covalent Organic Frameworks,*
First Edition. Omar M. Yaghi, Markus J. Kalmutzki, and Christian S. Diercks.

Companion website: www.wiley.com/go/yaghi/reticular

## 11.2 Top–Down Approach

One broadly applicable strategy to access thin films of COFs is to exfoliate crystallites of layered frameworks. Such structures are generally constructed from aromatic building units and an energy input is required to break up the strong π–π interactions between layers. This energy can be applied to the system by different means such as sonication or mechanical grinding. The advantage of these top–down approaches is that they are broadly applicable to a wide range of COFs as they do not have any specific requirements with respect to the structure or chemical composition of the material. Unfortunately, the thicknesses of the films obtained this way often show a broad size distribution. Alternatively, the layers in COF crystallites can be manipulated chemically by reaction with bulky substituents to set the layers apart and break the π–π interactions, an approach referred to as chemical exfoliation. Here, the advantage is that very thin films of uniform thickness can be obtained but the applicability of this approach is limited by the necessity for specific functionalities to carry out the chemical transformation inducing the exfoliation.

### 11.2.1 Sonication

Exposure of COF-43, a hydrazone-linked COF, to certain organic solvents leads to a substantial decrease in crystallinity (Figure 11.1a) [2]. This is surprising given the fact that based on chemical intuition, a hydrazone-linked framework should be stable under such conditions. It was found that samples of COF-43 exposed to organic solvents such as THF (tetrahydrofuran), chloroform, toluene, and MeOH (methanol) retained their crystallinity, while those exposed to dioxane, water, and DMF became amorphous. FT-IR spectra before and after solvent

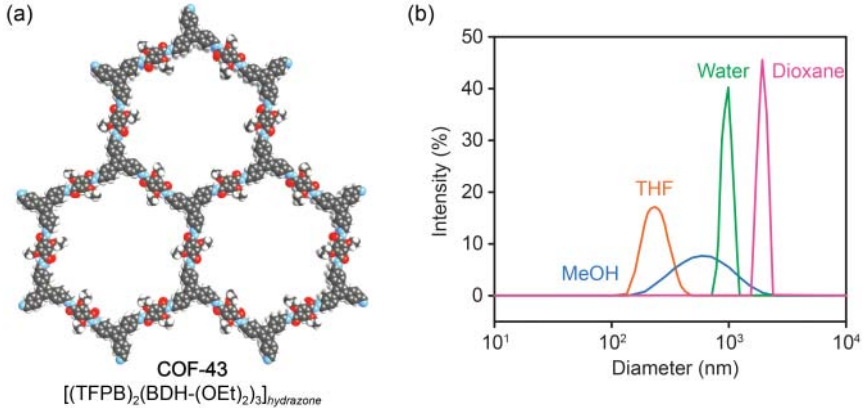


**Figure 11.1** (a) Structure of the mesoporous hydrazone-linked COF-43. (b) Average size of COF-43 dispersions derived from dynamic light scattering of solutions of microcrystalline COF-43 powder after brief sonication in THF, MeOH, water, and dioxane, respectively. Larger dispersed fragments are observed in exfoliating solvents (water, dioxane) as compared to non-exfoliating solvents (THF, MeOH). Color code for (a): H, white; C, black; N, blue; O, red.

exposure show that the characteristic C=O and C=N stretching vibrations at 1656 and 1597 $cm^{-1}$ of the hydrazone linkages are fully retained. The size of dispersed COF particles from different solvents, determined by dynamic light scattering (DLS), depends on whether the solvent induces apparent crystallinity loss. Atomic force microscopy (AFM) studies of COF particles from suspensions sonicated in dioxane indicate platelets with lateral widths of 200 nm and average heights of $1.32 \pm 0.37$ nm, corresponding to the thickness of 3–5 layers. More importantly, structures as thin as 3.3 Å are obtained from suspensions of COF-43 in water, corresponding to the formation of bi- or even single-layer structures. In contrast, COF suspensions in THF yield particles of morphologies similar to the as-synthesized COF powders. The size dependence of the COF particles from different organic solvents is illustrated in Figure 11.1b. TEM (transmission electron microscopy) confirms that the exfoliated layers retain their hexagonal symmetry and long-range order. The simplicity of this approach to the formation of COF thin films holds promise for large-scale fabrication from microcrystalline powders.

### 11.2.2 Grinding

The β-ketoenamine-linked **hcb** topology framework TPa-1 is prepared by reacting TFP with BDA. The resulting microcrystalline COF powder can be delaminated by grinding in a mortar for 30 minutes in the presence of a few drops of methanol. The powder of the delaminated COF can be suspended in methanol with concentrations of around 0.04 mg $mL^{-1}$ (~8 wt%) [3]. FT-IR spectra of the material show full retention of the characteristic C=O stretch and C–N stretch at 1580 and 1250 $cm^{-1}$, respectively. Powder X-ray diffraction (PXRD) patterns of the sheets corroborate that the integrity of the structure is fully retained, albeit with decreased intensity and broadening of the observed reflections. TEM images of the material show 100 nm to 1 μm thin graphene-like sheets. The laminar structure of the COFs was further assessed by AFM measurements, which reveal flat nanosheet-like structures with lengths and widths of several micrometers and thicknesses ranging from 3 to 10 nm. This corresponds to 10–30 COF layers, in good agreement with the TEM data. The advantage of mechanical grinding for the exfoliation of COFs is rooted in the notion that expensive organic solvents are not necessary to obtain the films.

### 11.2.3 Chemical Exfoliation

The anthracene-based $[(TFP)_2(DAA)_3]_{\beta\text{-}ketoenamine}$, is synthesized by the reticulation of linear ditopic DAA (2,6-diaminoanthracene) with trigonal tritopic TFP (2,4,6-triformylphloroglucinol). $[(TFP)_2(DAA)_3]_{\beta\text{-}ketoenamine}$ crystallizes in a **hcb** topology in the hexagonal space group $P6/mmm$ and features large 2.2 nm wide hexagonal channels along the crystallographic *c*-direction (Figure 11.2). The anthracene building units can post-synthetically be modified by [4+2]-Diels–Alder cycloaddition reactions with *N*-hexylmaleimide, thereby introducing bulky substituents between the individual COF layers to set them apart and delaminate the material [4]. Following the reaction by FT-IR shows

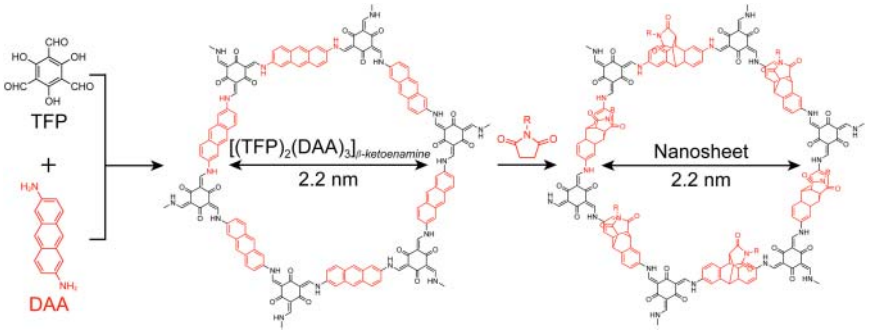


**Figure 11.2** Chemical delamination of the β-ketoenamine-linked $[(TFP)_2(DAA)_3]_{\beta\text{-}ketoenamine}$ by Diels–Alder reaction with *N*-hexylmaleimide. Illustrated are the chemical structure of $[(TFP)_2(DAA)_3]_{\beta\text{-}ketoenamine}$ and the reaction with *N*-hexylmaleimide to disrupt the π–π stacking between the layers and form the $[(TFP)_2(DAA)_3]_{\beta\text{-}ketoenamine}$ sheets. Only one pore is shown for clarity.

that the characteristic C=C and C–N stretching bands at 1590 and 1270 $cm^{-1}$ of $[(TFP)_2(DAA)_3]_{\beta\text{-}ketoenamine}$ are retained, while additional stretching bands at 2937 and 2857 $cm^{-1}$ corresponding to C–H vibrations arise from the *N*-hexyl groups of *N*-hexylmaleimide and the characteristic imide C=O bond stretch at 1695 $cm^{-1}$ of the maleimide itself. Analyses of the exfoliated sheets by scanning electron microscopy (SEM) demonstrate that the ribbon-like aggregated morphology of $[(TFP)_2(DAA)_3]_{\beta\text{-}ketoenamine}$ changes to micrometer-sized lateral rippled sheets. This phenomenon is also reflected in the TEM images, where $[(TFP)_2(DAA)_3]_{\beta\text{-}ketoenamine}$ again shows a ribbon-like morphology (100–200 nm in length, 20–40 nm in width). In contrast, the delaminated sheets exhibit a thin-sheet-like morphology (500 nm in width and 200 nm in thickness). The larger lateral feature size of the delaminated COFs is attributed to non-covalent interactions between small functionalized layers. AFM analysis of the delaminated $[(TFP)_2(DAA)_3]_{\beta\text{-}ketoenamine}$ shows an average thickness of about 17 nm. Owing to the presence of long alkyl chains and the resulting dipole interactions, the delaminated $[(TFP)_2(DAA)_3]_{\beta\text{-}ketoenamine}$ assembles into multilayer sheets with increased thickness. When the layers are suspended in dichloromethane and irradiated with a red laser ($\lambda = 650$ nm), a characteristic Tyndall effect is observed, indicative of single layer sheets in solution.

A scalable thin film composed of the delaminated $[(TFP)_2(DAA)_3]_{\beta\text{-}ketoenamine}$ can be obtained at the liquid–air interface. Toward this end, water is chosen as the liquid phase since the hydrophobic alkyl chains prevent the diffusion of the COF layers into the solvent. To fabricate a self-standing thin film, a suspension of delaminated $[(TFP)_2(DAA)_3]_{\beta\text{-}ketoenamine}$ in dichloromethane is added dropwise onto the water surface where it evaporates, leading to the formation of a semi-transparent thin film. TEM images show the aggregation of small nanosheets of 60–80 nm in width. The thickness of these films can be tuned from 1.2 to 1.6 nm (indicative of a single layer) up to 1.0–2.5 μm, by adjusting the concentration of the delaminated COF in the suspension. This high degree of control over the film

thickness down to a single monolayer renders chemical delamination a powerful approach for the formation of thin films of COFs.

## 11.3 Bottom–Up Approach

In contrast to top–down approaches, where the COF is first isolated as a microcrystalline powder and subsequently exfoliated to obtain nanostructured materials, bottom–up approaches have two significant advantages: (i) a higher degree of control over the feature size of the material, (ii) the potential for obtaining them in morphologies other than thin films, and (iii) the potential for direct interfacing with specific substrates. The big challenge in the bottom–up formation of nanostructured COFs is due to practical limitations with respect to the synthesis conditions employed. In Chapter 8 we have discussed the mechanism of bond formation for the various COF linkages that have been developed. It is important to consider that the mechanism of how these materials crystallize is much more complex than that. Understanding and manipulating the nucleation and subsequent seed growth during the crystallization of COFs is at the heart of controlling their morphology. Under conventional synthesis conditions COFs are isolated as aggregated microcrystalline powders and to obtain them as nanoparticles of different sizes or as films with uniform and controllable thickness several challenges need to be addressed. Conventional COF growth is generally carried out in suspensions rather than in homogeneous solutions. As a result, there is no control over the initial nucleation step and consequently particles of various sizes and shapes are obtained. To address this and figure out the parameters that need to be tuned to control the frameworks' morphology and feature size, the mechanism of COF crystallization needs to be deciphered. In the following, we will limit the discussion to frameworks constructed from boronate ester formation and reversible Schiff-base chemistry as for those linkages the crystallization mechanism has been thoroughly investigated.

### 11.3.1 Mechanism of Crystallization of Boronate Ester COFs

The mechanism of boronate ester COF formation has been studied for the case of COF-5. Homogeneous growth conditions were developed as opposed to the conventional reticulation of the starting materials from suspensions. The starting materials, HHTP and BDBA, for the formation of COF-5 are soluble in a 4 : 1 v/v mixture of dioxane/mesitylene with a small amount (15 equiv with respect to HHTP) of methanol in the reaction mixture. These homogeneous growth conditions enable the determination of the rate of precipitation of COF-5 by measuring the solution turbidity as a function of reaction time (Figure 11.3a). Under the homogeneous reaction conditions, a reproducible induction period during which soluble oligomers form and nucleation occurs is observed. After a few minutes at 90 °C, the crystalline COF starts to precipitate, at which point a change in the turbidity of the solution is recorded.

To test whether the reaction occurs reversibly a monofunctional catechol competitor, 4-(*tert*-butyl)benzene-1,2-diol, is added (Figure 11.3c). The addition,

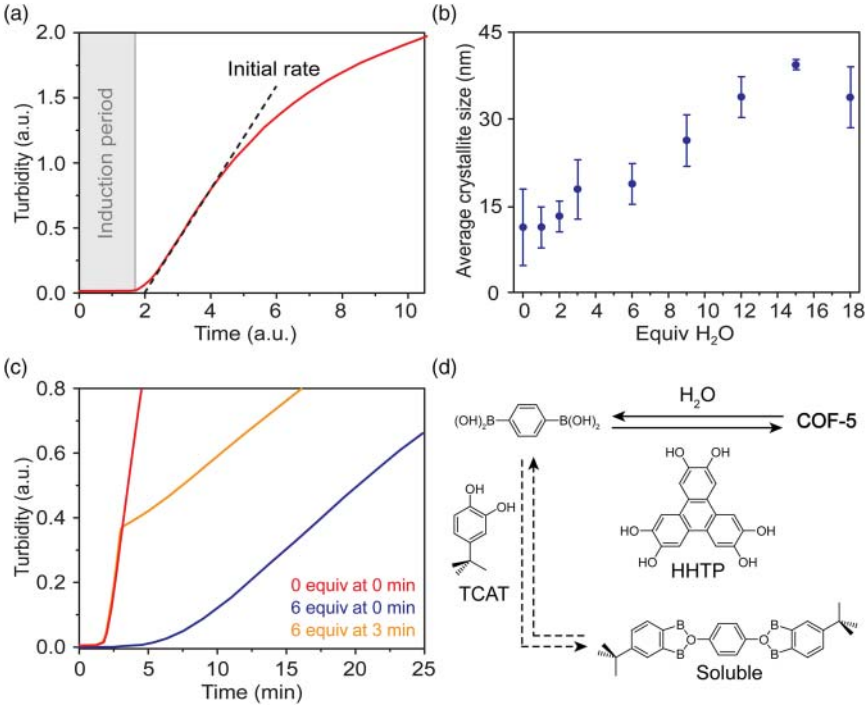


**Figure 11.3** Mechanistic studies for the formation of the boronate ester-linked framework COF-5. The system is tested under homogeneous reaction conditions starting from HHTP and BDBA in a 4 : 1 v/v mixture of dioxane/mesitylene. 15 equiv of methanol with respect to HHTP are added to enhance solubility. (a) The reaction occurs after an initial induction period. (b) Addition of water slows down the reaction but also increases the average crystallite size of COF-5. (c) This induction period is prolonged by addition of the monofunctional catechol competitor, *o*-cresol, at the beginning of the reaction. Addition at a later time, where the COF has already partially precipitated, does not result in re-dissolution of the framework but slows down further COF formation. (d) The experiments indicate that in the crystallization mechanism the mono-catechol competitor TCAT slows down the reaction by reversibly competing for the starting materials but does not participate in the reaction equilibrium. Water slows down the reaction by actively modulating the COF-forming equilibrium and this increased reversibility improves the crystallinity of the sample.

even in large excess, slows down but does not inhibit the reaction. This fact, in conjunction with the observation that the modulator is not incorporated into the final product, implies reversible bond formation at the early stages of the reaction. Addition of the modulator after partial precipitation of the COF slows down the formation of additional product but does not redissolve already formed crystallites, suggesting reversibility only in the early stages of seed growth and the existence of an irreversible step further down the crystallization/precipitation pathway. The addition of water (which is known to hydrolyze boronate ester COFs) to the reaction mixture also slows down COF formation, but in contrast to the addition of *o*-cresol, has a profound impact on the crystallite size (Figure 11.3b). By varying the amount of water added to the solution, the average crystallite size is doubled as determined by applying

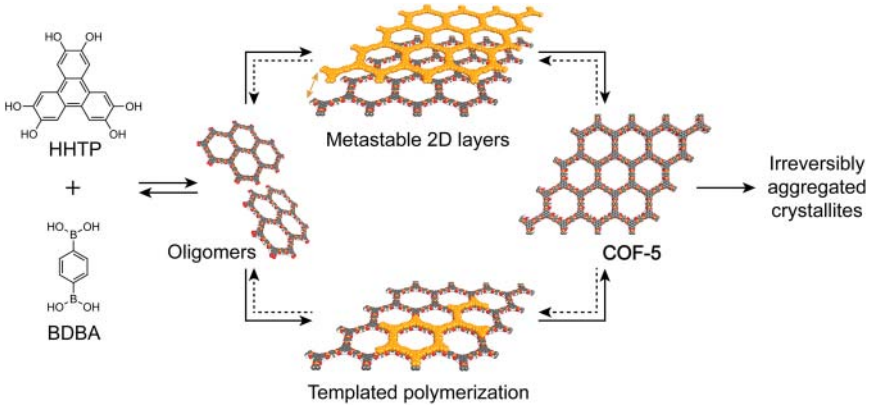


**Figure 11.4** Mechanism of the formation of COF-5. In a first reversible step HHTP and BDBA react and form soluble oligomers in solution. COF layers are formed upon further reaction. These metastable layers either stack with other layers or serve as nucleation sites for templated polymerization. The products of this step are colloidal COF-5 crystals. In a last irreversible step, individual COF-5 crystallites aggregate and precipitate from solution. COF-5 layers are partially highlighted in orange for clarity. Color code: H, white; B, orange; C, gray; O, red.

the Scherrer equation to the reflections observed in the powder patterns of the resulting COF. Taking stock of these findings, a mechanism for the formation of COF-5 can be proposed (Figure 11.3d). In the first step, small oligomers form from the starting materials in solution in a reversible manner. These oligomers function as seeds for the subsequent reversible growth of individual COF sheets. After formation of these sheets the material grows into individual COF crystallites in a reversible manner and subsequently aggregates and precipitates, at which point the material is withdrawn from equilibrium. This last irreversible step can be reversed to a certain extent by the addition of water and concomitant partial framework hydrolysis (Figure 11.4) [5].

#### 11.3.1.1 Solution Growth on Substrates

Based on the mechanism of boronate ester COF formation, the first challenge that needs to be addressed with respect to processing is to control the crystallite nucleation. A strategy to preferentially nucleate and thus control the growth of COF thin films makes use of substrates composed of single-layer graphene (SLG) supported on $SiO_2$ or copper wavers (Figure 11.5). The substrates are added as preferred nucleation sites to favor the formation of COF films on the SLG supported $SiO_2$ over random nucleation and crystallite growth in solution. For the formation of COF-5 thin films the substrates are directly added to the COF-forming reaction containing BPDA and HHTP. GIWAXS (grazing incidence wide angle X-ray scattering) shows that the layered films grow with preferred orientation of the layers normal to the SLG surface, which can be rationalized based on the maximized π–π interactions in this arrangement. The coverage and thickness of the films on the SLG surface are evaluated using SEM. A top–down micrograph of the COF films grown on SLG/Cu for 30 minutes indicates complete coverage of the graphene surface. A few bulk crystallites

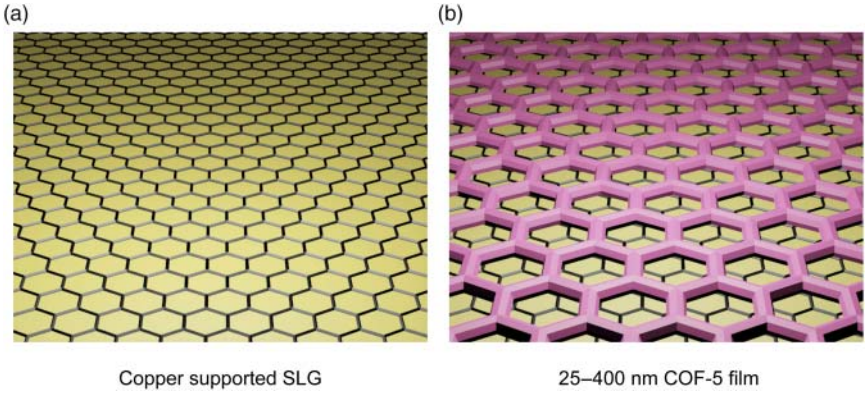


**Figure 11.5** Formation of COF-5 on a copper supported single layer graphene substrate. (a) Illustration of the copper supported single layer graphene. (b) Oriented thin films form where the COF layers crystallize parallel to the graphene sheet with a thickness of 195 ± 20 nm. Color code: Cu, gold; graphene, black; COF-5, pink.

are scattered on top of the film but can mostly be removed by sonicating the substrate in dry toluene for 10 seconds, after which the films are uniform over approximately 100 $mm^2$ areas. The cross section of a film grown for 30 minutes has a uniform thickness of 195 ± 20 nm, which corresponds to approximately 580 layers of COF. The limitations of this approach toward the bottom–up formation of boronate ester-linked COFs is the lack of control over the COF nucleation in solution resulting in the formation of aggregated crystallites that precipitate, some of which end up on the substrate thus resulting in less uniform films [6].

#### 11.3.1.2 Seeded Growth of Colloidal Nanocrystals

The mechanism of boronate ester COF formation implies that the precipitation of the framework from solution is due to irreversible agglomeration of individual crystallites. These crystallites are on the order of 100 nm in diameter and if their aggregation was prevented they could be processed as colloids from solution. Circumventing the precipitation requires the determination of conditions under which polymerization occurs but aggregation is inhibited. The addition of different amounts of nitrile solvents such as acetonitrile or benzonitrile results in stable colloidal suspensions of COF-5 where aggregation does not take place. The average particle size and polydispersity index for the colloids was determined for reaction mixtures of varying monomer and acetonitrile concentrations after reaction at 90 °C for 20 hours. For the tested concentrations of acetonitrile between 15 and 95 vol% the colloids exhibit Gaussian size distributions and low polydispersity indices. The average particle size is invariant at 45–60 nm for acetonitrile concentrations higher than 55%, which suggests stabilization of discrete crystallites at high acetonitrile concentrations. Larger colloids of dimensions between 100 and 240 nm are observed at 15 and 35 vol% acetonitrile, respectively, likely due to the aggregation of smaller crystallites. Once formed, the COF-5 colloids are stable for more than a month. Notably, the size of the colloids does not change

with time and can also not be modified by further addition of acetonitrile, indicating that once formed the particles are kinetically inert without appreciable monomer exchange. Unlike COF-5 in microcrystalline form, the colloidal solution is readily processable by evaporation of the solvent, and free-standing films of 10 μm in thickness can be obtained, which retain both the crystallinity and porosity of the parent material [7].

Making use of conditions where aggregation and precipitation are circumvented, stable colloids can function as seeds for further growth of larger single-crystalline COF particles. This is achieved when 80% of acetonitrile is included as a cosolvent in the COF-5-forming reaction to yield a COF-5 dispersion with colloids of 30 nm in size. Fast addition of monomers to this colloidal solution results in limited growth of the seeds and instead in new nucleation sites. This is supported by DLS measurements where the average crystallite size of the colloid decreases. In contrast, slow addition of the monomers favors the growth of existing colloids and only limited new nucleation is observed (Figure 11.6).

When the monomers are added slowly at a rate of 0.10 equiv $h^{-1}$ seeded growth dominates and the average particle size increases. The particle size can be increased from 400 nm to 1 μm upon addition of 4.0 equiv of starting materials. Notably, the size distribution of crystallites as determined by DLS remains monodisperse. Addition of the monomers at a higher rate of 1.0 equiv $h^{-1}$ results in an apparent decrease in the average particle size and a bimodal size distribution

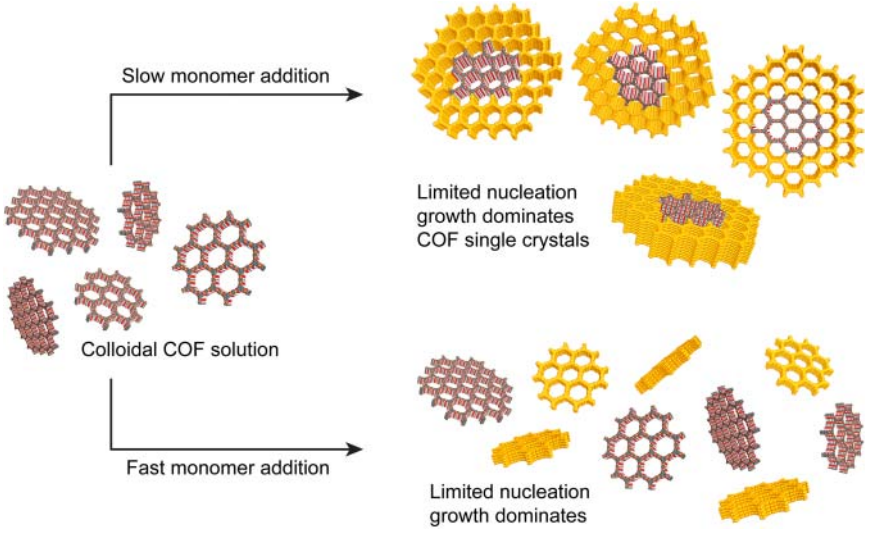


**Figure 11.6** Mechanism of seeded growth of COF-5 single crystals. A stable colloidal solution of COF-5 is obtained in reaction mixtures containing organic nitriles such as acetonitrile as solvents. Fast addition of monomers to this colloidal solution favors growth of the existing particles over new nucleation and consequently the particle size of COF-5 crystals is increased up to 1.5 μm. In contrast, when the monomers are added at a higher rate, new nucleation in solution dominates and limits the growth of existing particles. COF-5 formed upon further addition of monomers is highlighted in orange. Color code: H, white; B, orange; C, gray; O, red.

of particles, indicative of newly formed seeds upon addition of starting materials. The particles grown by this seeded growth approach are single crystalline as characterized by TEM but no unambiguous structure solution was reported.

#### 11.3.1.3 Thin Film Growth in Flow

One of the biggest challenges in the formation of COF thin films is the precise control over the film thickness. A protocol that allows incremental adjustment of film thickness is to grow them in flow and monitor the deposition using a quartz crystal microbalance (QCM). The formation of COF-5 and isoreticular analogs was studied by reacting HHTP with 1,4-phenyldiboronic acid (PDA) and expanded versions thereof. The reaction is run under homogeneous growth conditions, which is a necessary requirement for implementation into a flow cell setup. Under these conditions the induction period before precipitation of the framework is two minutes (Figure 11.7b). Accordingly, the length of the tubing needs to be adjusted in such a way that the material reaches the flow cell after two minutes to avoid clogging. By flowing the solution of reactants over the substrate a continuous deposition of mass with time is observed by applying the Sauebrey equation to the frequency response of the QCM (Figure 11.7a). This continuous increase in mass deposition goes along with an increase in resistance, further corroborating the continuous deposition of COF on the substrate. The deposited films are crystalline as evidenced by grazing incidence wide angle X-ray (GIWAX) scattering measurements, and the observed diffraction patterns are in good agreement with the proposed structural models. SEM images show continuous defect-free films without adhering crystallites. Films between 15 and 110 nm are made in a highly controllable manner as confirmed by AFM imaging [8].

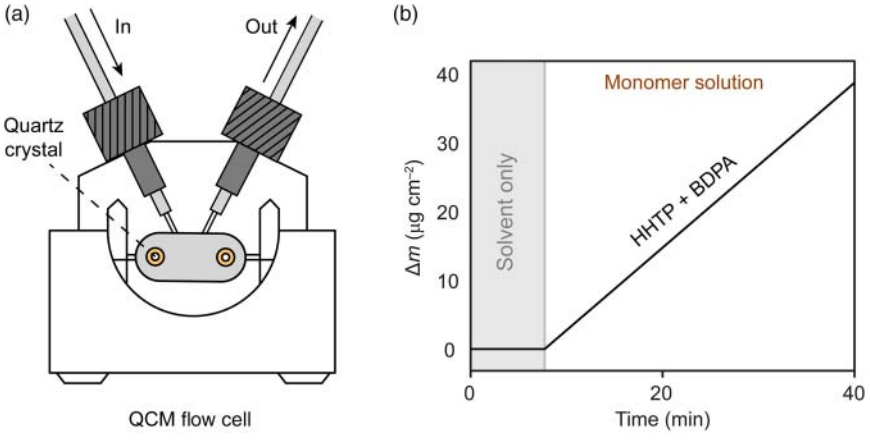


**Figure 11.7** Growing films of COF-5 using flow chemistry. (a) Illustration of a flow cell equipped with a quartz crystal microbalance (QCM) used in the experiment to follow the mass deposition of COF (left). (b) Change in mass of COF-5 formed from a solution of HHTP and BDPA in the heated flow cell as a function of the deposition time as determined by QCM measurements.

#### 11.3.1.4 Thin Film Formation by Vapor-Assisted Conversion

Another approach to growing thin films of COFs with a high level of control over the thickness is based on the application of steam-assisted conversion. Here, the idea is that the starting materials are processed into the desired morphology and only then be converted into the COF. Inherently, this approach cannot be carried out in solution. Alternatively, the starting materials are exposed only to vapor of solvents to prevent dissolution and loss of their preprocessed morphology. In practice, HHTP and BDA are dissolved in a mixture of acetone and ethanol and drop cast on a clean glass substrate. This glass substrate is subsequently placed into a desiccator along with a small vessel containing mesitylene and dioxane in a 1 : 1 v/v ratio. To achieve full conversion, the desiccator is stored for 72 hours at room temperature to yield evenly covered films of COF on the glass slides. SEM shows that the films are composed of small intergrown particles forming a continuous coverage on the substrate. Cross-sectional SEM reveals film thicknesses of 300 nm to 7.5 μm depending on the concentration of the precursor solution. PXRD of the films confirms the formation of COF-5 in crystalline form. To verify whether the films are porous, krypton sorption at 77.3 K was carried out after activation of the films at 150 °C under dynamic vacuum yielding a surface area of 990 $m^2 g^{-1}$. TEM micrographs of the polycrystalline COF films display the expected hexagonal honeycomb structure. This method holds promise for the formation of thin films due to the synthetic ease with which the films can be formed [9].

### 11.3.2 Mechanism of Imine COF Formation

For imine-linked COFs, a vastly different growth mechanism is observed, and we will illustrate this for the mesoporous **hcb** COF$[(TAPB)_2(BDA)_3]_{imine}$ (Figure 11.9). Homogeneous conditions are achieved in a mixture of 4 : 1 v/v dioxane/mesitylene. In contrast to the boronate ester-linked COF-5, which requires heating for the reaction to occur and shows an induction period of several minutes after which the material precipitates, no reaction occurs for $[(TAPB)_2(BDA)_3]_{imine}$ even when heating. When glacial acetic acid is added as a catalyst the reaction proceeds within seconds at room temperature but the resulting material is amorphous. Since the imine bond formation is a condensation reaction the influence of water on the crystallinity was tested and it was found that when both glacial acetic acid and water are added the initially amorphous precipitate transforms into a crystalline material over the course of two days (Figure 11.8a).

Based on these observations a reaction mechanism was proposed in which in the first step, an amorphous polyimine network forms, which over time slowly transforms into the targeted crystalline COF by reversible bond formation and concomitant error correction (Figure 11.8b). The different reaction mechanisms for boronate ester COFs and imine COFs imply that precipitated polyimine can still undergo reversible error correction, while boronate ester COFs precipitate irreversibly and directly in crystalline form (Figure 11.9). This is corroborated by the fact that for imine COFs linker exchange reactions are well established

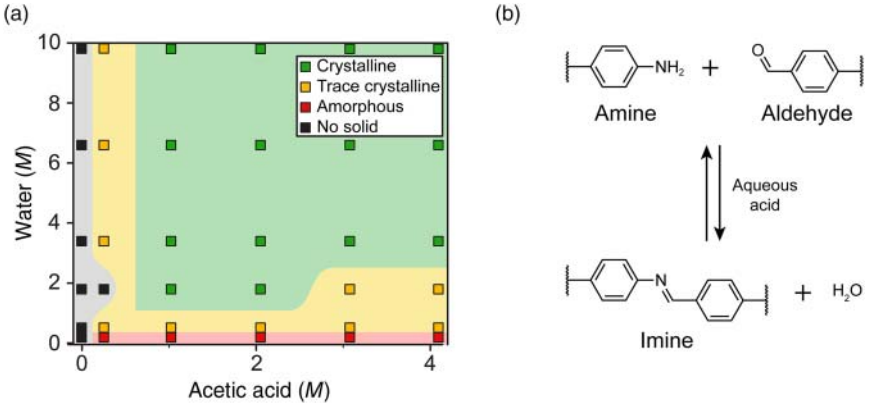


**Figure 11.8** Mechanistic studies for the formation of the imine-linked framework TPB-TP-COF. In a 4 : 1 v/v mixture of dioxane/mesitylene at 70 °C the reaction occurs homogeneously. (a) The influence of the addition of water and acetic acid shows that without addition of acetic acid no solid is formed. In contrast, no addition of water results in the formation of amorphous solid. By tuning the amount of both acid and water, crystalline material can be obtained. (b) With respect to the mechanism of COF formation it is concluded that both acid and water have to be added to the reaction mixture. While the acid serves as a catalyst to speed up the reaction, the water modulates the equilibrium between the starting materials and the product.

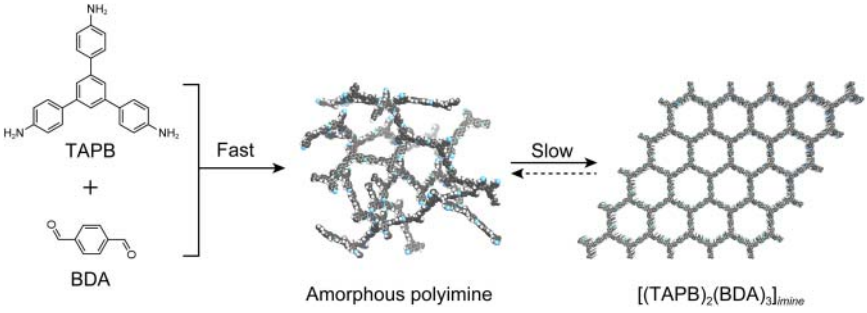


**Figure 11.9** Mechanism of $[(TAPB)_2(BDA)_3]_{imine}$ formation. In a first step, TAPB and BDA rapidly react to form an amorphous polyimine network. In a second slow step, the amorphous polymer is transformed into the crystalline COF by reversible bond formation and concomitant error correction. Color code: H, white; C, gray; N, blue.

whereas this has not been reported for boronate ester COFs [10]. The fundamental difference between the two mechanisms is that boronate ester COFs precipitate in crystalline form; their crystallization and precipitation occur simultaneously. For imine COFs the challenge in nanostructuring is that the crystallization and precipitation step occur separately. As a consequence, the strategies used for controlling the morphology of imine COFs are fundamentally different from the ones applied to boronate ester COFs.

#### 11.3.2.1 Nanoparticles of Imine COFs

As discussed earlier, the crystallization of imine COFs is a two-step process where at first an amorphous polyimine forms, which is subsequently converted into a

crystalline COF. In practice, both of these steps are usually achieved in a one-pot reaction. However, under the conditions that are required for the COF to crystallize, the polyimine formation is too rapid to effectively control nucleation. One approach to circumvent this issue is to divide the COF crystallization into two separate steps. For the formation of polyimines homogeneous growth conditions have been identified where the nucleation is prolonged and can thus be controlled more effectively through the addition of specific nucleation seeds into the reaction mixture. We have described this approach in Chapter 10 in the context of growing COFs around metal-oxide nanoparticles. When TAPB is reacted with TFB under homogeneous conditions in the absence of water the growth of the polymer proceeds slowly and exclusively on the surface of these added nucleation sites. 9.8 nm $Fe_3O_4$ nanoparticles, 9.0 nm Au nanoparticles, or 3.3 nm Pd nanoparticles were shown to serve as nucleation sites in this process. The second crystallization step is carried out under regular COF forming conditions and in the presence of acetic acid to yield the respective nanoparticles enclosed in 100 nm spheres of $[(TAPB)(TFB)]_{imine}$. This approach is useful because it represents a facile strategy for interfacing COFs with various other substrates. Furthermore, due to the controlled nucleation process it is in theory possible to control the thickness of the COF layer by adjusting the reaction time or the concentration of starting materials. However, using this approach, the nucleation of COFs only works in the presence of a substrate, which decreases the generality of the approach [11].

In order to address this shortcoming a different approach has to be taken. Instead of running the reaction in two consecutive steps, the initial nucleation period must be slowed down compared to the rate of error correction. In order to control the nucleation process the reaction intermediates need to be readily soluble. Toward this goal, partially Boc-protected (Boc, *tert*-butyloxycarbonyl) amine linkers are employed in COF synthesis. These linkers are slowly deprotected *in situ* thereby slowing down the polymerization step, whereas the rate of error correction remains unaltered. The formation of LZU-1 is carried out under homogeneous conditions when NBPDA(4-(*tert*-butoxycarbonylamino)-aniline) is used (instead of 1,4-benzene diamine) and reacted with TFP (1,3,5-trisformylphenyl benzene) in ethanol as the solvent. TFA (trifluoro-acetic acid) is used as a catalyst and PVP (polyvinylpyrolidone) as a capping agent. In the homogenized imine COF synthesis, nuclei form from clear solution and grow into crystalline frameworks before precipitation. In a typical synthesis, NBPDA and TFB are dissolved in ethanol in the presence of PVP and TFA, and subsequently heated at 120 °C for 30 minutes to yield a red suspension of protonated LZU-1 nanocrystals. This suspension immediately turns yellow upon deprotonation with an ethanol/triethylamine solution. The fact that the COF is protonated during the synthesis is crucial since this renders the nanocrystals polar and allows for PVP to bind and passivate their surface thus regulating the growth in alcoholic solution. The size and morphology of the crystallites were characterized by SEM revealing an average size of $245 \pm 25$ nm. The size of the LZU-1 nanocrystals can conveniently be tuned by varying the concentration of PVP. Addition of 5 mg $mL^{-1}$ of PVP yields COF particles of $500 \pm 52$ nm in size and 40 mg $mL^{-1}$ of PVP gives crystals of $112 \pm 11$ nm. The

COF particles form colloidal solutions in ethanol and remain stable for weeks. The importance of the solvent in the crystallization process is supported by the fact that the morphology of COF nanocrystals strongly correlates with solvent composition. In particular, the addition of toluene to the ethanol solution results in crystallites of distinctly hexagonal shape. This morphology strongly supports the proposed homogeneous nature of the crystal growth process and highlights the high crystallinity of the resulting materials [12].

#### 11.3.2.2 Thin Films of Imine COFs at the Liquid–Liquid Interface

The nucleation of imine COFs takes place only in the presence of acid catalyst. This is exploited to grow COFs at the liquid–liquid interface by interfacing a solution of the COF starting materials in organic media with an aqueous layer containing the acid catalyst. Imine COF formation generally relies on high temperatures to ensure reversibility. This is detrimental in the case of interfacial growth where high reaction temperatures disturb the interface resulting in inhomogeneous films. Furthermore, acetic acid, commonly used as the catalyst in imine COF formation, is readily soluble in organic solvents rendering the formation of a defined interface difficult. Lewis acidic metal triflates can catalyze the imine bond formation, even at room temperature. In the formation of $[(TAPB)_2(BDA)_3]_{imine}$ from TAPB and BDA a series of metal triflates were investigated as potential catalysts. The addition of $In(OTf)_3$ (OTf, triflate) and $Sc(OTf)_3$ was found to lead to crystalline COFs in as little time as one minute at room temperature (Table 11.1) [13].

The advantage of Lewis acidic metal triflate catalysts is that they are readily soluble in water but not soluble in a lot of organic solvents. This, in combination with the fact that they operate at room temperature, allows for the formation of imine COFs at the liquid/liquid interface. When $Sc(OTf)_2$ (0.001 equiv) is applied as a catalyst in the aqueous layer and TATB and BDA are dissolved in a 1 : 4 v/v mixture of mesitylene/dioxane, the COF-forming reaction occurs exclusively at the interface between both solvents since all three reagents are

**Table 11.1** Enumeration of catalysts for imine bond formation for the case of $[(TAPB)_2(BDA)_3]_{imine}$.

| Entry | Catalyst | T/°C | RT/min | Isolated yield (%) |
|---|---|---|---|---|
| 1 | $In(OTf)_3$ | 20 | 1 | 95 |
| 2 | $Sc(OTf)_3$ | 20 | 5 | 98 |
| 3 | $Yb(OTf)_3$ | 20 | 10 | 98 |
| 4 | $Y(OTf)_3$ | 20 | 30 | 96 |
| 5 | $Eu(OTf)_3$ | 20 | 60 | 98 |
| 6 | $Zn(OTf)_3$ | 20 | 150 | 95 |
| 7 | $CH_3COOH$ | 20 | N/A | 0 |

The reaction rates and isolated yields for metal triflates and acetic acid are compared at 20 °C; RT = reaction time, N/A = not avaliable.

required for imine condensations to occur at room temperature. The reaction proceeds over the course of 72 hours and control over the thickness of the films (20 nm to 100 μm) is achieved by controlling the monomer concentration in the organic layer, as confirmed by AFM. PXRD patterns of the films are consistent with the proposed structural model of the COF. For very thin films the diffraction intensity is too low for PXRD and TEM and the crystallinity cannot be confirmed unambiguously [14].

## 11.4 Monolayer Formation of Boroxine and Imine COFs Under Ultrahigh Vacuum

A different approach is taken for the formation of COF monolayers under ultrahigh vacuum. Early reports of a monolayer of COF grown this way were achieved by chemical vapor deposition of BDA under ultrahigh vacuum and at 370 K onto a Ag(111) surface. Annealing of the sample results in the formation of the expected structure, COF-1, which can be followed using STM (scanning tunneling microscopy) at room temperature [15]. The small feature size of the resulting material is attributed to the lack of reversibility of the reaction due to water leaving the equilibrium under the ultrahigh vacuum conditions. To address this issue, a small amount of $[Cu(SO_4)]\cdot 5H_2O$ is added to the reaction, which is carried out on a highly ordered pyrolytic graphite (HOPG) surface and in a sealed system. The $[Cu(SO_4)]\cdot 5H_2O$ acts as a water reservoir in order to regulate the chemical equilibrium of the dehydration reaction, resulting in highly ordered networks. The water molecules released from $[Cu(SO_4)]\cdot 5H_2O$ during the heating process shift the equilibrium back to promote error correction under reversible reaction conditions, a necessary requirement for the formation of high-quality films. Upon cooling back to room temperature, the water released from $[Cu(SO_4)]\cdot 5H_2O$ is reabsorbed by the anhydrous $[Cu(SO_4)]$ formed, thus preventing the potential decomposition of the COF film due to dehydration of the boroxine linkage. In addition to the formation of COF-1, this strategy was successfully applied to construct two COFs with different pore sizes by self-condensation of 9,9′-dihexylfluorene-2,7-diboronic acid and 4,4′-biphenyl-diboronic acid. All three frameworks show long-range periodicity and negligible amounts of defects. It was shown that this strategy can further be applied to the formation of imine-linked COFs. Both the cross-condensation of TAPB with BDA and the reaction of TFP (1,3,5-trisformylbenzene) with PDA (1,4-benzenediamine) result in a monolayer of $[(TAPB)_2(BDA)_3]_{imine}$ and LZU-1, respectively. Both materials feature long-range periodicity as evidenced by STM images of the material [16].

## 11.5 Summary

In this chapter, we covered the top–down and bottom–up approaches for the nanoscopic and macroscopic structuring of COFs. Layered COF crystallites

can be exfoliated into single/few layer sheets or thin films of the material. This requires an energy input that can be derived from mechanical forces (grinding, sonication) or can be the result of chemical alteration of the structure (chemical exfoliation). Bottom–up approaches for structuring of COFs require a detailed understanding of the crystallization pathway, which in turn is dependent on the linkage chemistry used to construct the framework. We have covered, in detail, the crystallization mechanisms for imine and boronate ester-linked COFs. By making use of the rate-determining steps of the crystallization or by manipulation of these steps COFs can be isolated as stable nano-sized colloids, micron-sized single crystals or as thin films. In the context of thin film formation of COFs we have introduced different techniques: film formation by controlled nucleation on substrates, nucleation at the liquid–liquid interface, growth in a flow cell, vapor-assisted conversion, and the formation of single COF layers under ultrahigh vacuum. Finally, we have highlighted which COF linkages are amenable to which structuring methodologies based on their underlying crystallization mechanisms.

## References


1 (a) Wan, S., Gándara, F., Asano, A. et al. (2011). Covalent organic frameworks with high charge carrier mobility. *Chemistry of Materials* 23 (18): 4094–4097. (b) DeBlase, C.R., Silberstein, K.E., Truong, T.-T. et al. (2013). β-Ketoenamine-linked covalent organic frameworks capable of pseudocapacitive energy storage. *Journal of the American Chemical Society* 135 (45): 16821–16824. (c) Lin, S., Diercks, C.S., Zhang, Y.-B. et al. (2015). Covalent organic frameworks comprising cobalt porphyrins for catalytic $CO_2$ reduction in water. *Science* 349 (6253): 1208–1213.

2 (a) Uribe-Romo, F.J., Doonan, C.J., Furukawa, H. et al. (2011). Crystalline covalent organic frameworks with hydrazone linkages. *Journal of the American Chemical Society* 133 (30): 11478–11481. (b) Bunck, D.N. and Dichtel, W.R. (2013). Bulk synthesis of exfoliated two-dimensional polymers using hydrazone-linked covalent organic frameworks. *Journal of the American Chemical Society* 135 (40): 14952–14955.

3 Chandra, S., Kandambeth, S., Biswal, B.P. et al. (2013). Chemically stable multilayered covalent organic nanosheets from covalent organic frameworks via mechanical delamination. *Journal of the American Chemical Society* 135 (47): 17853–17861.

4 Khayum, M.A., Kandambeth, S., Mitra, S. et al. (2016). Chemically delaminated free-standing ultrathin covalent organic nanosheets. *Angewandte Chemie International Edition* 55 (50): 15604–15608.

5 (a) Smith, B.J. and Dichtel, W.R. (2014). Mechanistic studies of two-dimensional covalent organic frameworks rapidly polymerized from initially homogenous conditions. *Journal of the American Chemical Society* 136 (24): 8783–8789. (b) Li, H., Chavez, A.D., Li, H. et al. (2017). Nucleation and growth of covalent organic frameworks from solution: the example of COF-5. *Journal of the American Chemical Society* 139 (45): 16310–16318. (c) Koo, B., Heden, R., and Clancy, P. (2017). Nucleation and growth of 2D covalent

organic frameworks: polymerization and crystallization of COF monomers. *Physical Chemistry Chemical Physics* 19 (15): 9745–9754.

6 (a) Colson, J.W., Woll, A.R., Mukherjee, A. et al. (2011). Oriented 2D covalent organic framework thin films on single-layer graphene. *Science* 332 (6026): 228–231. (b) Cote, A.P., Benin, A.I., Ockwig, N.W. et al. (2005). Porous, crystalline, covalent organic frameworks. *Science* 310 (5751): 1166–1170.

7 Smith, B.J., Parent, L.R., Overholts, A.C. et al. (2017). Colloidal covalent organic frameworks. *ACS Central Science* 3 (1): 58–65.

8 Bisbey, R.P., DeBlase, C.R., Smith, B.J., and Dichtel, W.R. (2016). Two-dimensional covalent organic framework thin films grown in flow. *Journal of the American Chemical Society* 138 (36): 11433–11436.

9 Medina, D.D., Rotter, J.M., Hu, Y. et al. (2015). Room temperature synthesis of covalent–organic framework films through vapor-assisted conversion. *Journal of the American Chemical Society* 137 (3): 1016–1019.

10 (a) Smith, B.J., Overholts, A.C., Hwang, N., and Dichtel, W.R. (2016). Insight into the crystallization of amorphous imine-linked polymer networks to 2D covalent organic frameworks. *Chemical Communications* 52 (18): 3690–3693. (b) Qian, C., Qi, Q.-Y., Jiang, G.-F. et al. (2017). Toward covalent organic frameworks bearing three different kinds of pores: the strategy for construction and COF-to-COF transformation via heterogeneous linker exchange. *Journal of the American Chemical Society* 139 (19): 6736–6743.

11 Rodríguez-San-Miguel, D., Yazdi, A., Guillerm, V. et al. (2017). Confining functional nanoparticles into colloidal imine-based COF spheres by a sequential encapsulation-crystallization method. *Chemistry - A European Journal* 23 (36): 8623–8627.

12 (a) Zhao, Y., Guo, L., Gándara, F. et al. (2017). A synthetic route for crystals of woven structures, uniform nanocrystals, and thin films of imine covalent organic frameworks. *Journal of the American Chemical Society* 139 (37): 13166–13172. (b) Ding, S.-Y., Gao, J., Wang, Q. et al. (2011). Construction of covalent organic framework for catalysis: Pd/COF-LZU1 in Suzuki–Miyaura coupling reaction. *Journal of the American Chemical Society* 133 (49): 19816–19822.

13 Matsumoto, M., Dasari, R.R., Ji, W. et al. (2017). Rapid, low temperature formation of imine-linked covalent organic frameworks catalyzed by metal triflates. *Journal of the American Chemical Society* 139 (14): 4999–5002.

14 Matsumoto, M., Valentino, L., Stiehl, G.M. et al. (2018). Lewis-acid-catalyzed interfacial polymerization of covalent organic framework films. *Chem* 4 (2): 308–317.

15 Zwaneveld, N.A., Pawlak, R., Abel, M. et al. (2008). Organized formation of 2D extended covalent organic frameworks at surfaces. *Journal of the American Chemical Society* 130 (21): 6678–6679.

16 (a) Liu, X.-H., Guan, C.-Z., Ding, S.-Y. et al. (2013). On-surface synthesis of single-layered two-dimensional covalent organic frameworks via solid–vapor interface reactions. *Journal of the American Chemical Society* 135 (28): 10470–10474. (b) Guan, C.-Z., Wang, D., and Wan, L.-J. (2012). Construction and repair of highly ordered 2D covalent networks by chemical equilibrium regulation. *Chemical Communications* 48 (24): 2943–2945.